DOI: 10.1002/cbic.200700750

Cellular Dynamics of Ku: Characterization and Purification of Ku-eGFP

Dennis Merkle,*[b] Dan Zheng,[c] Thomas Ohrt,[a] Karin Crell,[a] and Petra Schwille*[a]

Ku is a predominantly nuclear protein that functions as a DNA double-strand-break (DSB) binding protein and regulatory subunit of the DNA-dependent protein kinase (DNA-PK). DNA-PK is involved in synapsis and remodeling of broken DNA ends during nonhomologous end-joining (NHEJ) of DNA DSBs. It has also recently been demonstrated that Ku plays roles in cytoplasmic and membrane processes, namely: interaction with matrix metalloproteinase 9, acting as a co-receptor for parvoviral infection, and also interacting with cell polarity protein, Par3. We present a method for creating stable expression of Ku-eGFP in CHO cells and extend the procedure to purify Ku-eGFP for in vitro assaying. We demonstrated that Ku-eGFP localizes to the nucleus of HeLa cells upon microinjection into the cytoplasm as well as localizing to laser induced DNA damage. We also characterized the diffusional dynamics of Ku in the nucleus and in the cytoplasm using fluorescence correlation spectroscopy (FCS). The FCS data suggest that whereas the majority of Ku (70%) in the nucleus is mobile and freely diffusing, in a cellular context, there also exists a significant slow process fraction (30%). Strikingly, in the cytoplasm, this immobile/slow moving fraction is even more pronounced (45%).

Introduction

The Ku heterodimer, consisting of Ku70 and Ku80, was originally identified as an autoantigen recognized in the sera of patients with autoimmune disease. Cells that lack either Ku70 or Ku80 undergo premature senescence, are radiosensitive and defective in DNA double-strand-break (DSB) repair. Animals lacking Ku manifest numerous phenotypes including growth defects, radiosensitivity, and immunodeficiency.[1] Ku is predominantly a nuclear protein with high affinity for DSBs in vitro and in vivo (reviewed in ref. [2]). Crystallographic analysis of Ku has revealed that both subunits contribute to a cradle-like structure that completely encircles the DNA double helix, much like a bead on a string.[3] As a regulatory component of the DNA-dependent protein kinase (DNA-PK), Ku is important for facilitating the repair of DSBs by nonhomologous end joining (NHEJ). It is postulated that during the initial steps of NHEJ, Ku binds the DSB termini and subsequently recruits and activates the catalytic subunit of DNA-PK (DNA-PKcs). Autophosphorylation of the active DNA-PK holoenzyme facilitates end processing, termini alignment, and ultimately ligation.[2]

Recently, the less abundant cytoplasmic population of Ku has gained interest. Expressed on the surface of a subset of cells, Ku contributes to cell–cell adhesion and the migration process of activated monocytes.[4] It has been demonstrated to function with matrix metalloproteinase 9 to facilitate cell adhesion with fibronectin[5,6] and also serves as co-receptor for human parvovirus B19 infection, regulating viral entry into target cells.[7]

The past decade has seen great advances in the implementation of fluorescence techniques. Fluorescence correlation spectroscopy (FCS), fluorescence resonance energy transfer (FRET), and fluorescence recovery after photobleaching (FRAP), among others, have become increasingly popular to study protein, lipid, small ligand, and DNA dynamics both in vitro and in vivo. Researchers examining NHEJ have directly applied many of the above mentioned fluorescence techniques to elucidate how the various molecular players in the pathway interact and function.[8–12] Although only beginning to be understood, the role of Ku within the cytoplasm is clearly highly divergent from its well-established role within NHEJ and the nucleus. To date, no clearly evident fundamental differences between nuclear and cytoplasmic Ku have been observed. To gain insight into the potentially differential properties of Ku within the nucleus and cytoplasm, we performed a biophysical analysis of eGFP-tagged Ku expressed in mammalian cells. Both in vitro and in vivo, eGFP-Ku conforms to the anticipated activity of functional Ku. Using fluorescence correlation spectroscopy (FCS) to assess the diffusional dynamics of Ku, we find that cytoplasmic Ku is substantially less mobile than its nuclear counterpart, suggesting that it is actively constrained.

[a] *Dr. T. Ohrt, K. Crell, Prof. Dr. P. Schwille*
Institute of Biophysics, Biotechnology Center
Dresden University of Technology
Tatzberg 47–49, 01307 Dresden (Germany)
Fax: (+49) 351-463-40342
E-mail: petra.schwille@biotec.tu-dresden.de

[b] *Dr. D. Merkle*[+]
Current address: Philips Research
High Tech Campus 11, 5656 AE Eindhoven (The Netherlands)
Fax: (+31) 40-2749244
E-mail: dennis.merkle@philips.com

[c] *D. Zheng*[+]
Current address: ETH Zürich, HPT D52
Wolfgang-Pauli-Strasse 16, 8093 Zürich (Switzerland)

[+] *These authors contributed equally to this work.*

Results

Stable transfection of human Ku80-eGFP in CHO XrS6 cells

We transfected CHO XrS6 cells with a construct for human Ku80 fused to eGFP. The resulting cells expressed eGFP fluorescence stably and showed an expected predominant nuclear localization, indicative of Ku (Figure 1 A). In contrast, CHO XrS6 cells transfected with eGFP alone demonstrated a homogeneous cellular distribution (no preference for nuclear or cytoplasmic localization), and could not be stably maintained (see Figure 5 D and E, below). To verify that the eGFP was fused to Ku80 we performed an immunoblot against Ku80, Ku70 (Figure 1 B), and eGFP (Figure 1 C) from whole cell extracts of wild-type (wt) CHO, CHO XrS6, and CHO XrS6-Ku80eGFP cells. Immunoblot analysis revealed the fusion of eGFP to Ku80 by an observed and characteristic shift in molecular weight of approximately 30 kDa (the size of eGFP) in the Ku80 band within the CHO XrS6-Ku80eGFP cells (ca. 116 kDa), as compared to the wt Ku80 appearing with the expected 86 kDa size (Figure 1 B). In addition, it has been demonstrated that in the absence of Ku80, the Ku70 subunit is unstable in vivo (and vise versa).[13,14] Immunoblot analysis revealed that Ku70 was stabilized in the XrS6-Ku80eGFP cells to a similar degree as wt CHO cells versus the nontransfected XrS6 cells (Figure 1 B). In addition, we examined the same extracts by immunoblot with respect to eGFP. Both CHO wt and CHO XrS6 cells were negative for eGFP, whereas the CHO XrS6-Ku80eGFP cell line did cross-react with the anti-eGFP antibody (Figure 1 C). As a control we loaded purified eGFP alone into a well, which was also recognized in the eGFP immunoblot. It can be seen that the eGFP in the CHO XrS6-Ku80eGFP cells is indicative of Ku80-eGFP fusion protein with a shifted molecular weight at approximately 116 kDa (corresponding well with the position of the band from the Ku80 immunoblot), versus the band at approximately 30 kDa for eGFP alone. Taken together, these results demonstrate that Ku80eGFP is expressed in the CHO XrS6 cell line and this expression leads to the stabilization of Ku70.

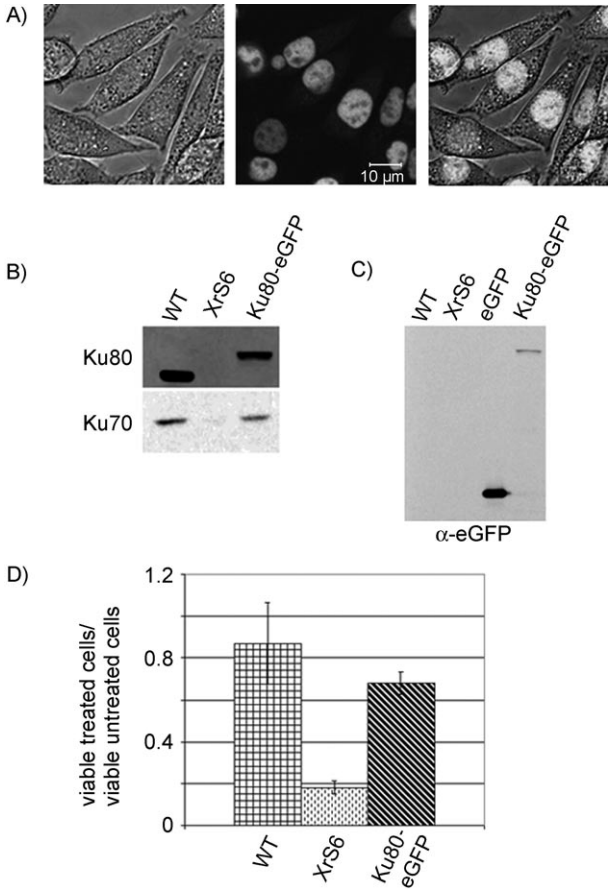

Figure 1. CHO XrS6 cells stably express Ku80eGFP. A) Laser scanning microscope images of Ku-eGFP expressing cells shown in phase contrast (left), 509 nm fluorescence (middle), and merged (right). Scale bars are 10 μm. B) Immunoblots against Ku80 and Ku70 in whole cell extracts from wt CHO, XrS6, and XrS6-Ku80eGFP transfected cells. C) Immunoblot against eGFP from whole cell extracts of wt CHO, XrS6, and XrS6-Ku80eGFP transfected cells, as well as, purified eGFP. α is an abbreviation for an immunoblot with antibody directed against, in this case eGFP. D) wt CHO, XrS6, and XrS6-Ku80eGFP cells were treated with 2.5 μM of etoposide for 1 h and then incubated in fresh media for 48 h. Cells were then stained with trypan blue and counted. Ratios are expressed on the *y*-axis as a total number of viable etoposide treated cells versus the viable cell count from the same line treated with a corresponding amount of DMSO as a control.

Cells lacking either Ku subunit, such as the Ku80 deficient CHO XrS6 line, are deficient in the repair of DNA DSBs. It has been shown that complementing XrS6 cells with human Ku80 rescues this DSB repair-deficient phenotype[15–17] and we next wanted to verify that complementation of XrS6 cells with our Ku80eGFP construct also rescued DNA DSB sensitivity in the stable transfected cells. We assessed the survival of wt CHO, CHO XrS6, and CHO XrS6-Ku80eGFP cells with respect to recovery after DNA DSB induction with etoposide. Etoposide is a chemotherapeutic compound known to cause DNA DSBs in cells via topoisomerase II inhibition.[18] Cells were treated with etoposide (2.5 μM) for one hour, washed, and incubated for 48 hours in fresh medium. After two days, viable cells were counted and compared to DMSO controls. Figure 1 D displays the results of the survival assay. It is clear that XrS6 cell survival is severely compromised after DNA DSB induction as compared to CHO wt (approximately 20% compared to wt cell survival). In contrast, the XrS6-Ku80eGFP cells showed a marked recovery in survival after etoposide treatment (approximately 80% compared to wt CHO cell survival). These results indicate that we have created a stable cell line expressing functional Ku-eGFP and we next sought to purify the intact hamster Ku70/human Ku80eGFP heterodimer.

Purification of Ku-eGFP heterodimer

Ku-eGFP was purified to an approximate homogeneity of >95% from stably transfected XrS6-Ku80eGFP cells (8.4 L; see the Experimental Section; Figure 2 A). The protocol required at least four chromatographic stages and yielded approximately 23μg of stable Ku-eGFP. Ku70 and Ku80eGFP coeluted at all stages of purification and Ku-eGFP had a high affinity for DNA

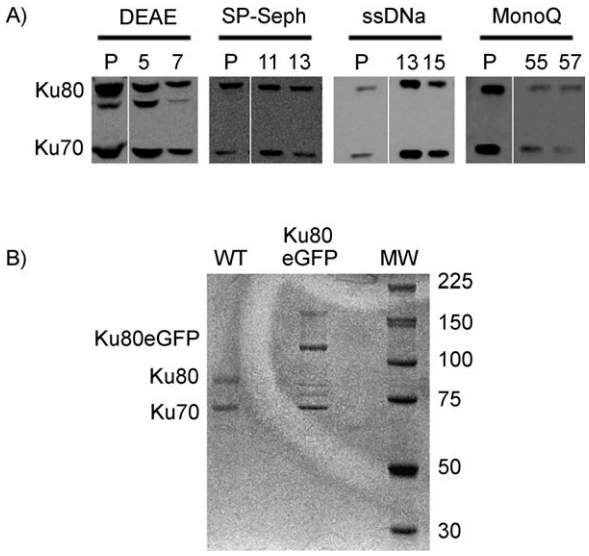

Figure 2. Purification of Ku-eGFP. A) Immunoblots against Ku70 and Ku80 during each stage of the purification procedure. P = prefraction, whereas the numbers indicate the two peak fractions from each column elution. B) Coomassie blue stain of purified Ku-eGFP next to that of purified wild-type human Ku heterodimer. MW = molecular weight marker, with each number indicative of the molecular weight of each corresponding band.

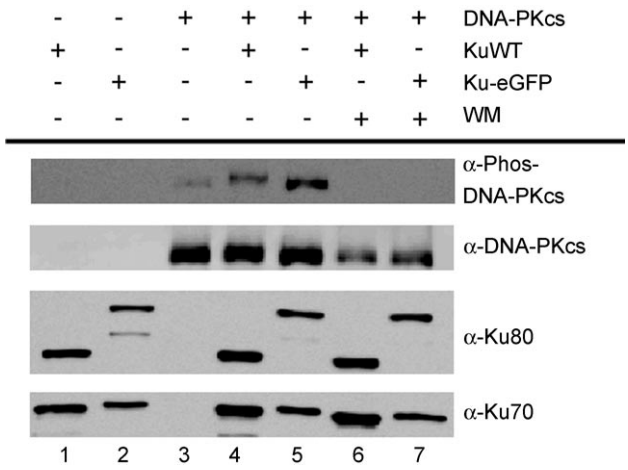

Figure 3. Ku-eGFP is capable of stimulating DNA-PK autophosphorylation at threonine 2609. Immunoblots against Ku70, Ku80, DNA-PKcs, and DNA-PKcs-PhosphoThr2609 (α is an abbreviation for immunoblot with antibody directed against the listed respective proteins). All reactions were performed under kinase reaction conditions, containing CT-DNA and Mg-ATP. Lane 1: wt Ku alone. Lane 2: Ku-eGFP alone. Lane 3: DNA-PKcs alone. Lane 4: DNA-PKcs + wt Ku. Lane 5: DNA-PKcs + Ku-eGFP. Lane 6: DNA-PKcs + wt Ku + WM. Lane 7: DNA-PKcs + Ku-eGFP + WM. WM = wortmannin.

cellulose. The purified heterodimer contained equimolar ratios of Ku70 and Ku80-eGFP, as judged by Coomassie staining.

Ku-eGFP stimulates DNA-PK autophosphorylation at threonine 2609

It has been shown that in vitro DNA-PKcs has weak kinase activity that is stimulated approximately tenfold upon the addition of Ku in vitro.[19,20] In vivo, it is clear that DNA-PK activity and recruitment is dependent upon the presence of Ku.[12] The primary substrate of DNA-PK is DNA-PKcs itself, and so we examined the ability of our Ku-eGFP to support DNA-PKcs autophosphorylation. DNA-PK autophosphorylation was assessed (see the Experimental Section) using either purified Ku or Ku-eGFP. Both the endogenously expressed Ku and Ku-eGFP supported DNA-PKcs autophosphorylation to a similar degree; this indicated that the eGFP tag did not affect the ability of Ku to bind DNA and recruit and activate DNA-PK (Figure 3). As a control we also demonstrated that Ku-eGFP-stimulated DNA-PK activity was also inhibited by the fungal metabolite, wortmannin, a well-characterized PI3-kinase (and DNA-PK) inhibitor (Figure 3).[12]

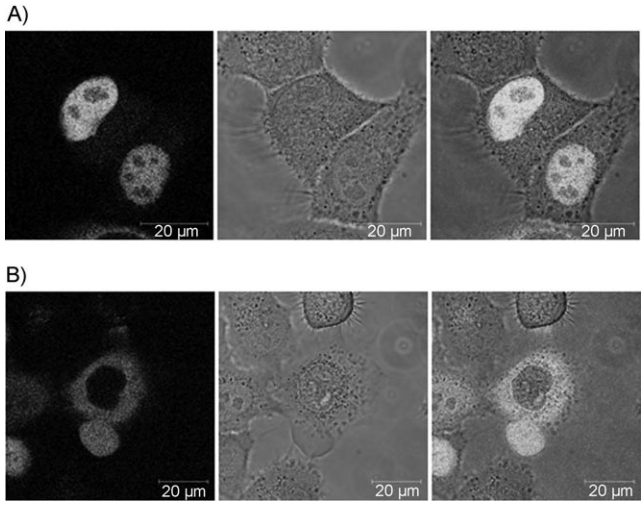

Figure 4. Microinjected Ku-eGFP into the cytoplasm of HeLa cells localizes to the nucleus. Ku-eGFP was microinjected into A) healthy growing and B) dead HeLa SS6 cells. Within minutes the Ku-eGFP 509 nm emission was predominantly localized to the nucleus in the living cell (A) whereas the nuclear translocation to the nucleus of the dead cell was impaired (B). Left panels are phase contrast images, middle panels are 509 nm fluorescence images, and right panels are merged images. Scale bars are 20 μm.

Nuclear localization of microinjected Ku-eGFP in HeLa cells

Nuclear localization signals (NLSs) in Ku have been shown to mediate transport into the nucleus.[21,22] Indeed, we observed a clear nuclear localization preference for the stable transfected CHO XrS6-Ku80eGFP cells (Figure 1). In order to test whether the hamster/human hybrid Ku-eGFP also preferentially localizes to the nucleus in human cells, the purified Ku-eGFP was microinjected into the cytoplasm of HeLa SS6 cells (Figure 4). Within minutes, Ku-eGFP was located predominantly in the cell nucleus (Figure 4A). Ku-eGFP did not enter the nucleolus in both CHO and HeLa cells (shown as dim circular stained nuclear features, Figures 1A and 4A). As a comparison, microinjected Ku-eGFP in the cytoplasm of dead cells did not localize to the nucleus, presumably because of impaired nuclear transport (Figure 4B, notice the large bleb).

Ku-eGFP localization to laser induced DNA damage in cells

It has been demonstrated that a focused, pulsing laser can be a potent inducer of DNA DSBs in vivo.[9,11,12,23] Herein, we used a two-photon laser to produce DNA DSBs in both the stable transfected Ku-eGFP CHO cells and the Ku-eGFP microinjected HeLa cells described above (Figure 5). Cells were cut linearly such that no obvious cellular damage could be visualized with DIC optics on the microscope (data not shown). In contrast, fluorescence imaging revealed a bright green "stripe" appearing along the laser track representing the accumulation of Ku-eGFP at sites of DNA damage (Figure 5A, C, and F). Both control experiments on CHO cells transfected with eGFP alone (nuclear and cytoplasmic, Figure 5D and E) or laser damage in the XrS6-Ku80eGFP cell cytoplasm (Figure 5B) did not indicate any localization of the eGFP fluorescence to the laser track. Taken together, these results demonstrate that the hamster Ku70/human Ku80eGFP heterodimer is capable of localizing to laser induced DNA damage in both hamster and human cells, and that this localization is nucleus specific (that is, DNA-dependent) and not an eGFP artifact or due to mass cellular laser damage.

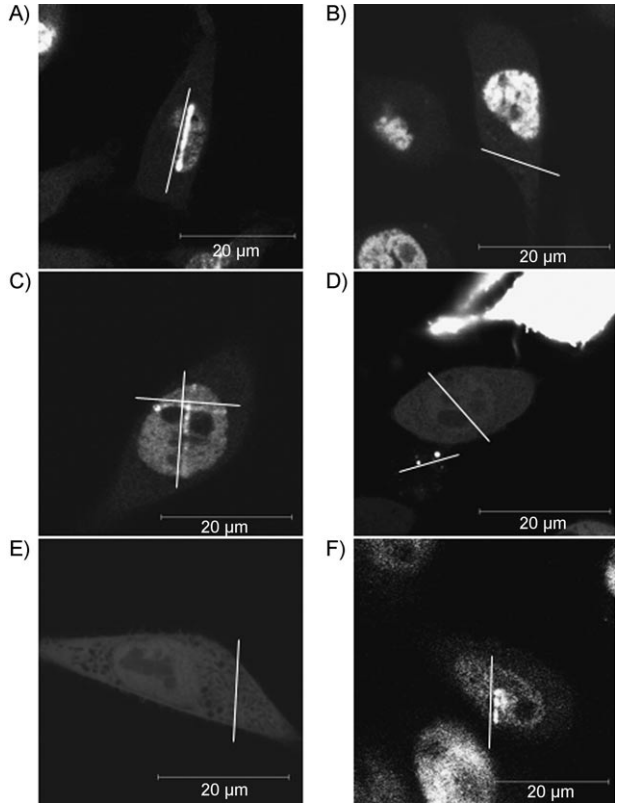

Figure 5. Ku-eGFP localizes to DNA damage induced by a pulsed two-photon laser in both XrS6-Ku80eGFP cells and Ku-eGFP-microinjected HeLa SS6 cells. A) and C) Laser tracks across the nucleus of Ku-eGFP expressing XrS6 cells. White lines are set as a guide of the laser track and were placed approximately parallel and next to the actual laser track. Panel A demonstrates a single track, and in Panel C a "cross-hair" was tracked. B) Laser track through the cytoplasm of an XrS6-Ku80eGFP cell shows no Ku-eGFP localization. D) Laser track through the nucleus of eGFP expressing XrS6 cells does not result in eGFP localization to the laser path. E) Laser track through the cytoplasm of eGFP expressing XrS6 cells does not result in eGFP localization to the laser path. F) Laser track through the nucleus of a Ku-eGFP microinjected HeLa SS6 cells results in Ku-eGFP localization to the laser path.

Fluorescence correlation spectroscopy for the characterization of Ku-eGFP diffusion

Finally, we sought to examine the diffusion dynamics of Ku-eGFP in the cell nucleus and in the cytoplasm using fluorescence correlation spectroscopy. As a control, these experiments were performed in unison with cells transfected with only eGFP. Figure 6 shows typical FCS curves obtained in XrS6 cells for A) Ku-eGFP and B) eGFP for both the nucleus (dashed lines) and the cytoplasm (solid lines). Fits of the data confirmed previous observations for eGFP dynamics in cells, specifically, we observed an average diffusion coefficient for eGFP of $(2.75\pm0.42)\times10^{-11}\ m^2s^{-1}$ ($n=8$) in the nucleus and $(2.93\pm0.37)\times10^{-11}\ m^2s^{-1}$ ($n=6$) in the cytoplasm. These "fast" diffusing fractions were predominant in the order of $87\pm5\%$ ($n=14$) of the diffusing species, whereas there also existed a "slow process" component of approximately 13%. We applied the same two component fit parameters to the XrS6-Ku80eGFP cells yielding diffusion coefficients for Ku-eGFP of the order of $(1.43\pm0.11)\times10^{-11}\ m^2s^{-1}$ ($n=15$) for the nucleus and $(1.38\pm0.15)\times10^{-11}\ m^2s^{-1}$ ($n=15$) for the cytoplasm. Interesting was the presence of a significant "slow process" fraction. The fast diffusing component of Ku-eGFP in the nucleus was a clear majority of $70\pm6\%$ ($n=15$) versus a significant, but smaller, $30\pm6\%$ ($n=15$) slow fraction diffusing at a rate of $(7.96\pm1.22)\times10^{-13}\ m^2s^{-1}$ ($n=15$). In contrast, the cytoplasmic Ku-eGFP had approximately equal amounts of fast and slow moving components, with the fast fraction consisting of approximately $55\pm2\%$ ($n=15$) versus an approximate $45\pm2\%$ slow moving fraction diffusing at a rate of $(6.47\pm1.62)\times10^{-13}\ m^2s^{-1}$ ($n=15$). In solution, the purified Ku-eGFP diffused at a rate of $(2.12\pm0.36)\times10^{-11}\ m^2s^{-1}$ ($n=3$), an expected decrease in diffusion times when comparing globular protein diffusion in cells to that in buffered solution.[24,25] Accordingly, we observed a diffusion coefficient of purified eGFP in solution at approximately $7–7.5\times10^{-11}\ m^2s^{-1}$ (data not shown) versus $2.8–2.9\times10^{-11}\ m^2s^{-1}$ in vivo.

Discussion

In this study we describe the establishment of a stable transfected Ku80eGFP cell line, including an efficient procedure for the purification of Ku-eGFP heterodimer. We purified the hybrid human Ku80eGFP/hamster Ku70 to approximately $>95\%$ with a final yield of 23 μg from an initial cell pellet of a confluent 8.4L culture. The protocol used herein was heavily based upon previously published papers for Ku from human placenta and HeLa cells.[20,26] The purified Ku-eGFP was capable of stimulating DNA-PKcs autophosphorylation at threonine 2609, a site shown to be phosphorylated in vivo as a response to ionizing radiation (IR) induced DNA DSBs,[27] as effectively as wild-type Ku, indicating that the eGFP fusion does not significantly interfere with Ku-DNA binding, translocation, or DNA-PKcs interaction. We also characterized Ku-eGFP with respect to cellular localization to the nucleus, localization to laser in-

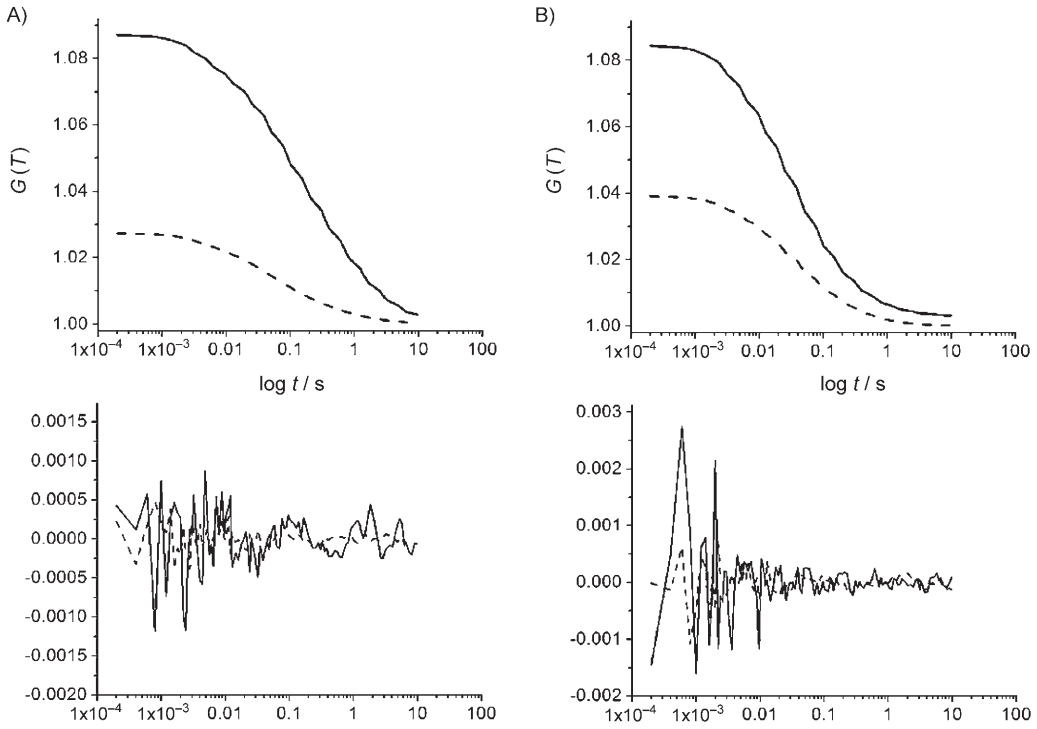

Figure 6. Typical FCS curves and corresponding fit residuals for Ku-eGFP and eGFP in CHO XrS6 cells. Figures represent fits of the raw data. Residuals of the data fits are shown in the lower panels. A) FCS curves of Ku-eGFP in the XrS6 nucleus (-----) and cytoplasm (——). Fitting of these data indicate that in the nucleus there is a 76% fast moving fraction at a diffusion coefficient of 1.42×10^{-11} m^2s^{-1} and a 24% slow process fraction, 9.41×10^{-13} m^2s^{-1}. The cytoplasmic Ku-eGFP is also in two fractions, a 57% mobile fraction (1.36×10^{-11} m^2s^{-1}) and a 43% immobile fraction (10.35×10^{-11} m^2s^{-1}). B) FCS curves of eGFP in the XrS6 nucleus (-----) and cytoplasm (——). Fitting of these data indicate that in the nucleus there was a predominant (>84%) mobile fraction with a diffusion time of 2.81×10^{-11} m^2s^{-1} whereas in the cytoplasm the fast component was also dominant (>86%) with a diffusion time of 2.99×10^{-11} m^2s^{-1}.

duced damage sites, and ability to rescue the DNA DSB deficiency inherent in the XrS6 cell line and all control experiments indicated that Ku-eGFP behaves as native Ku.

It has been demonstrated in several studies that DNA damage induced by lasers elicits the recruitment of a wide variety of NHEJ and DNA damage proteins, including Ku, to the "laser track" (i.e., the region of the nucleus illuminated with the laser beam.[9,11,12,23] In both our stable Ku80eGFP expressing cells and in the Ku-eGFP-microinjected HeLa SS6 cells this observation was consistent. The laser power used in the current study was of the order of 5 J per pulse with a beam radius of approximately 0.31 μm, comparable to powers and beam sizes (and hence comparable amounts of DNA damage, that is, 1000–1500 DNA breaks produced at the beam focus) used in the previous studies using a similar laser setup.[11] This results in Ku-eGFP localization to the laser track within seconds of irradiation (Figure 5). At very high laser powers one can severely damage the cell (i.e., burn a hole), and in our experiments we confirmed the absence of massive cellular damage with DIC optics, which can also distinguish "laser tracks" in the cytoplasm under high laser intensity settings (data not shown).

Most interesting was the examination of the Ku-eGFP diffusional behavior in the XrS6 cells with fluorescence correlation spectroscopy. FCS has become a popular, reliable, and sensitive technique for detailed examination of protein, lipid, and nucleic acid dynamics in vivo.[28–30] We observed a two component diffusion fit to the data representing; 1) a fast, mobile fraction of approximately $1.43–1.38\times10^{-11}$ m^2s^{-1} in both the nucleus and cytoplasm and 2) what we termed a "slow process" fraction of approximately $7.96–6.47\times10^{-13}$ m^2s^{-1} in the nucleus and cytoplasm. Although we do report herein the diffusion times of the slow fraction, the exact values are likely not significant because of limitations of FCS in examining such processes.[31–33] In order to examine such slow diffusing phenomena, one requires very long illumination times, and this can result in photoinduced artifacts.[31] This fact also makes it difficult to comment upon the exact cause of the slow process. That is, it may represent subcellular confinement and immobility of Ku, and/or dynamic processes such as binding and unbinding to membranes, chromatin, and/or cytoskeletal components (we are currently examining these in more detail). Nonetheless, the diffusion times observed for the mobile Ku-eGFP were very reasonable when compared to that of eGFP. There exists a direct relation between the ratio of molecular weights (M_W) of the two globular proteins and the ratio of their respective diffusion times (T_D) [Eq. (1)]:

$$[\tau_{D\text{-protein 1}}/\tau_{D\text{-protein 2}}] = [M_{W\text{protein 1}}/M_{W\text{protein 2}}]^{1/3} \quad (1)$$

The hydrodynamic radius is proportional to the cubic root of the volume, V_h (for a spherical particle), which in turn scales with the mass (m) of the particle (with the density (ρ)). For globular molecules, the hydrodynamic radius, R_h, is therefore proportional to the cubic root of the molecular mass. Thus, it

is possible to calculate the hydrodynamic radius if the viscosity and dimensions of the detection volume are known, or to estimate the mass of an unknown particle in relation to a protein of well-known mass.[34] The molecular weight of eGFP is approximately 30 kDa, and we characterized its cellular diffusion times at approximately 376 and 353 μs in the nucleus and cytoplasm respectively (calculated from the relation of the respective diffusion coefficients and the axial radius of the focal volume of our instrument, see the Experimental Section). Applying these values to Equation (1) with the diffusion times for Ku-eGFP in the nucleus and cytoplasm (725 and 750 μs, respectively), one would estimate a molecular weight for Ku-eGFP of approximately 215–288 kDa. These values are very reasonable compared to the expected 186 kDa MW of Ku-eGFP, within the error for our data and resolution limits for FCS.[35] The cell interior is a crowded and compact space, filled with various organelles and multiprotein complexes. The larger a protein is, the more confined the diffusion within the cell, and hence it is not surprising to see the Ku-eGFP diffusing in vivo at slower speeds. In solution it has been shown that the diffusion times of globular proteins are 3–10 times faster than in the cell.[25,36] We observed a faster diffusion time in buffer, approximately 488 μs, for Ku-eGFP, versus the approximate 725–750 μs diffusion time in vivo, however the effect may not be considered as drastic as expected (<3). Perhaps the 3D structure of the Ku heterodimer contributes to the diffusion, as the protein is shaped much like a basket (not ideally globular), with a broad base that cradles the DNA double helix through a small loop of polypeptide chains encircling the helix.[3] This basket-like structure may result in differing diffusional properties of the Ku-eGFP, with respect to eGFP alone. In addition, the DNA binding cradle of the Ku heterodimer possesses a positive charge, and hence may be prone to "stick" or interact with negatively charged cellular components.[3] Furthermore, if a portion of the diffusing Ku protein is interacting with other proteins (e.g., DNA-PKcs) this can also result in an observed slower mean diffusion.

Also interesting was the distributions of the fast and slow process fractions of Ku-eGFP in both the nucleus and cytoplasm. It has been shown that eGFP exists predominantly in a fast/free diffusing state (approximately 90%, in good agreement with our data)[25,36] whereas for Ku-eGFP both the cytoplasmic and nuclear slow process fractions were significant (ca. 30% and 45% respectively). This may suggest that approximately 30% of nuclear Ku could be immobilized (chromatin associated?). It has been shown that Ku plays critical roles in telomere maintenance and interacts directly with hTR, the RNA component of human telomerase. It has also been suggested that Ku can interact with certain transcriptional promoter regions.[37–39] These processes, along with endogenous DNA DSBs in an already highly condensed chromatin environment, may explain the observed slow components of the Ku diffusion. More striking is the 45% immobile fraction found in the cytoplasm. Ku has been shown to be present in the cytoplasm, albeit to a much lesser extent that in the nucleus.[40,41] However, recently it has been demonstrated that Ku interacts at the plasma membrane with matrix metalloproteinase 9 (MMP9)[5] and can interact with the cell polarity protein Par3, which is known to interact with actin.[42] In addition Ku has been shown to be a co-receptor for parvovirus cell infection and facilitate cell adhesion to fibronectin.[6,7] These studies have demonstrated a clear role for Ku outside the nucleus, and hence, whereas Ku is less abundant in the cytoplasm, it clearly plays critical roles in non-nuclear processes. Immobilization (or binding and unbinding) to cytoskeletal components and other slow diffusing or membrane-associated protein complexes may explain this high degree of the "slow" component in the FCS data.

FRAP has been previously used to examine the dynamics of nuclear Ku-eGFP and Ku-YFP in response to laser induced DNA damage.[9,11,12] These studies were primarily focused on Ku dynamics in the cell nucleus and do not provide a detailed analysis, quantification of diffusion coefficients, or distributions of fast and slow diffusing fractions. In addition these previous studies emphasized the kinetics of localization of Ku to laser induced DNA damage sites.[9,11,12] Nonetheless, it has been demonstrated that in the nucleus, the majority of Ku-eGFP is in a mobile fraction diffusing at more or less the same rate as other proteins of similar molecular weight (although no specific diffusion times were assigned).[11] This supports our observed diffusion coefficient of 1.43×10^{-11} m^2s^{-1} for Ku-eGFP in the nucleus, and the corresponding estimated molecular weight of 215 kDa from comparison to nuclear eGFP diffusion with Equation (1). Again, the most striking result we observed was that approximately 70% of the nuclear Ku is diffusing freely (in the context of the cell nucleus) whereas this mobile fraction significantly decreases to 55% in the cytoplasm. This highlights another advantage of FCS, as it is an incredibly sensitive technique (single molecule sensitivity) it can be used to access dynamics of low abundant species, such as cytoplasmic Ku.[28–30] In order to successfully apply FRAP, one needs a significant amount of fluorescence expression, and this may explain why FRAP studies on Ku were confined to the nucleus, where Ku is very abundant. It will be interesting to examine the dynamics of Ku diffusion in the nucleus and cytoplasm upon DNA DSB induction as well as the change in Ku dynamics upon cytoskeletal rearrangements. These experiments are currently in progress and will be elaborated upon in a future study. It should be noted that FCS can in theory also access subcellular concentrations (i.e., the $G(T)$ value is inversely proportional to the number of particles (n) diffusing within the focal volume). We did not report these values as there were variations in the amount of Ku-eGFP and eGFP expressed from one individual cell to another (this can be seen in the difference in fluorescence intensity of the two cell nuclei in the bottom left corner of Figure 1A, middle panel, and the two cells in Figure 5D, for example). Nonetheless it was clear from measurements on similar intensity cells that the nuclear fractions contained a higher abundance of Ku-eGFP than the cytoplasm, whereas this was not the case for the eGFP transfected cells (data not shown).

Conclusions

To summarize, we have demonstrated that Ku-eGFP is a powerful biophysical tool for the examination of NHEJ dynamics in

vivo and in vitro. In fact, a multitude of fluorescence biophysics studies of Ku have been successfully by applied using FRET to examine Ku translocation internally on DNA upon DNA-ligase IV/Xrcc4 binding,[8] FCS and FCCS (fluorescence cross-correlation spectroscopy) to examine phosphorylation-dependent DNA-PK complex associations in solution,[10] fluorescence anisotropy to examine the effects of salt ions on Ku–DNA interactions in solution,[43] and FRAP to study the dynamics of Ku-DSB localization in the cell nucleus.[9,11,12] We also present an efficient protocol for the isolation of Ku-eGFP and demonstrate, for the first time, that it is functional in both in vitro and in vivo assays. Finally, we examined the dynamics of Ku-eGFP using FCS in vivo, for the first time, in both the cell nucleus and cytoplasm and demonstrate that microinjection of Ku-eGFP (and other fluorescence-labeled proteins, for that matter), can provide valuable insight into the dynamics of cellular localization.

Experimental Section

Materials: All salts and chemicals used, unless otherwise stated, were purchased from Sigma.

Cells and cell culture: Adherent HeLa SS6 cells were cultured in an 8.5% CO_2 humidified incubator at 37 °C in DMEM (Invitrogen, 41966) with fetal bovine serum (FBS; 10%, Cambrex, DE14-802F) and were regularly passaged at subconfluency. Adherent CHO K1 wt cells were cultured in Alpha-MEM (Invitrogen, 22571) supplemented with FBS (10%), CHO XrS6 cells were cultured in MEM (Sigma, M2279), supplemented with FBS (10%), MEM nonessential amino acids (Invitrogen, 1140–035), and L-glutamine (2 mM, Invitrogen, 25030–024). The stable transfected CHO XrS6-eGFP-Ku80 cell line was cultured as regular XrS6 with additional Geniticin (1 mg mL^{-1}, Invitrogen, 10131-027) as selection antibiotic. All CHO cells were incubated with 5% CO_2 and were regularly passaged at subconfluency.

For experiments with the cell lines mentioned, 6.0×10^4 cells mL^{-1} were transferred onto MatTek chambers coated with poly-D-lysine (0.1 mg mL^{-1} in PBS, P7280 Sigma) 24 h before microinjection. Cells were washed twice with air buffer [150 mM NaCl, 20 mM Hepes pH 7.4, 15 mM glucose, 5.4 mM KCl, 0.85 mM $MgSO_4$, 1.7 mM $CaCl_2$, 0.15 mg mL^{-1} BSA, 46 mM trehalose] and incubated in air buffer for 15 min prior to confocal imaging, FCS, or microinjection.

Ku80-eGFP plasmid generation: A pWay vector for the expression of full length human Ku70 and Ku80 fused to eGFP at the C terminus was a kind gift of Dr. W. Rodgers (Oklahoma Medical Research Foundation). Transfection of these plasmids could not be sustained stably. Instead Ku80 was amplified from the pWay20Ku80eGFP plasmid utilizing the expand high fidelity PCR system (Roche) with primers directed against Ku80: CTCAGATCTCCATGGTGCGGTCGGGGAAT and AAGGATCCCTATATCATGTCCAATAAATCGTCCA.

The purified Ku80 gene fragment was ligated into pGEM-T vector (Promega). Ku80-pGEM-T was electroporated into XL-1 Blue bacteria for amplification utilizing blue-white screening on LB agar plates with ampicillin, X-Gal + IPTG. Amplified Ku80-pGEM-T was purified with a miniprep plasmid DNA purification kit (Qiagen) and sequenced with T7 and SP6 primers.

Ku80-pGEM-T and pEGFP-C2 vectors (Clontech) were digested with Bg1II and BamHI (MBI Fermentas) and the pEGFP-C2 vector dephosphorylated with calf intestine alkaline phosphatase (Fermentas). The excised Ku80 gene fragment and the digested pEGFP-C2 vector were subsequently purified with a gel extraction kit (Qiagen). Finally, the Ku80 insert was ligated into the pEGFP-C2 vector using T4 DNA Ligase (NEB). The resulting pEGFP-C2-Ku80 plasmid was then electroporated into XL-Blue bacteria and plated on LB agar with kanamycin. Positive clones were selected for amplification and sequencing of the pEGFP-C2-Ku80 vector, used below to express Ku80eGFP (fused at the N-terminal end of Ku80).

Stable transfection of Ku80eGFP into CHO XrS6 cells: Circular pEGFP-C2-Ku80 plasmid was linearized with Eco31I (Fermentas) prior to transfection with Lipofectamine 2000 (Invitrogen). CHO XrS6 cells were seeded at 4×10^4 cells mL^{-1} in a six-well plate (Nunc) 24 h before transfection (reaching approximately 50% confluency). Transfection was carried out using linearized DNA (1150 ng per well) and lipofectamine (6 μL per well). All steps were carried out according to the manufacturer's specifications. After 4.5 h of incubation with the lipoplex solution at 37 °C and 5% CO_2, medium was exchanged to prevent toxic effects of the transfection reagent. Cells were trypsinized and seeded into T25 flasks (25 cm^2, Nunc) after 24 h, followed by addition of the selection antibiotic G418 after 48 h. Another passage of the cells was performed six days after transfection into T75 flasks (75 cm^2, Nunc), leading to subconfluency after three additional days, when cells were prepared for recloning in 96-well plates (Nunc). Fluorescent colonies derived by single cells within certain wells were trypsinized and seeded in 24-well plates and progressively subcultivated into six-well plates and T25 and T75 flasks. Positive clones were confirmed with PCR after cell lysis and by Western blot analysis (see below).

Cell survival assay: CHO wild type, CHO XrS6, and CHO XrS6-Ku80eGFP cells were seeded in six-well plates at 2×10^4 cells mL^{-1} (total of three wells per cell line, one for control purposes (DMSO), and two for etoposide treatment). Etoposide stock in DMSO (50 mM) was diluted in PBSM (to 500 μM) and subsequently added to the cells in fresh medium (at a final concentration of 2.5 μM). For controls, the remaining wells were incubated with an equivalent concentration of DMSO. Cells were incubated at 37 °C and 5% CO_2 for one hour followed by media removal, two washes with fresh medium (2 mL), and were subsequently incubated for 48 h. Finally the cells were trypsinized, resuspended in medium, and centrifuged at 200 g for 4 min. Cell pellets were resuspended in PBSM (200 μL) and treated with Trypan blue (0.1 mL of 0.4% Trypan Blue Stain) for 2 min at room temperature. Total and dead (blue stained) cells from each well were counted in a hemocytometer. The total number of viable cells from each well was determined by subtracting the number of dead cells from the total cell count. The cell survival assay was expressed as a ratio of viable cells in the etoposide treated wells divided by the number of viable cells in the corresponding DMSO control wells, for each cell line; CHO wt, CHO XrS6, and CHO XrS6-Ku80eGFP.

Purification of Ku-eGFP: CHO XrS6-Ku80eGFP cells (8.4 L) were cultured to confluence as described above. The cells were trypsinized, resuspended in PBS containing FBS (10%), and centrifuged (5 min, 200 *g*, 4 °C). The pellet was washed once with PBS, once with low salt buffer [LSB: 10 mM Hepes pH 7.4, 25 mM KCl, 10 mM NaCl, 1 mM MgCl2, 0.1 mM EDTA], then resuspended in twice the packed cell volume of LSB containing protease inhibitors and DTT. Extract was snap frozen in liquid nitrogen and stored at −80 °C until further purification. From this point on, all buffers used contained a cocktail of DTT (0.1 mM), PMSF (0.2 mM), pepstatin A (0.1 μg mL^{-1}), and Benzamidine (0.1 mM).

Frozen cell pellets (37 mL) were thawed and extracted with high salt buffer [HSB: 20 mM Tris-HCl pH 8.0, 5 M NaCl, 100 mM $MgCl_2$, 0.1 mM EDTA, 10 mM DTT] (to a final concentration of 500 mM NaCl), incubated on ice for 15 min, and centrifuged at 30000 *g* for 25 min at 4 °C. The supernatant was removed and stored on ice. Protein concentrations were determined using a NanoDrop ND-1000 spectrophotometer. Unless otherwise stated, all subsequent steps were carried out at 4 °C.

The supernatant (27.5 mL) was dialyzed against tris buffer with KCl (75 mM; TB/75 mM KCl) until the conductivity was equivalent. The sample (total protein 388.75 mg) was applied to a Ø2.5 cm×8 cm DEAE-Sepharose fast flow (Amersham Biosciences) equilibrated in TB/75 mM KCl. The column was washed with TB/75 mM KCl, and sequentially eluted with TB/175 mM KCl and TB/750 mM KCl. Ku-eGFP eluted in the TB/175 mM KCl fractions (20 fractions of 10 mL). The presence of Ku-eGFP in column fractions was resolved by SDS-PAGE and immunoblotting.

Ku-eGFP-containing fractions from the DEAE column (total protein 56.4 mg) were pooled, dialyzed against TB/75 mM KCl, and applied to a ø1.5 cm×8 cm column of SP-Sepharose fast flow (Amersham Biosciences) equilibrated in TB/75 mM KCl. The SP-Sepharose column was washed with TB/75 mM KCl, and sequentially eluted with TB/175 mM KCl and TB/750 mM KCl. Ku-eGFP eluted in the TB/175 mM KCl fractions (70 fractions of 1–1.5 mL). The presence of eGFP-Ku in column fractions was resolved by SDS-PAGE, immunoblotting, and Coomassie blue staining.

Ku-eGFP-containing fractions from SP-Sepharose column (total protein 4.83 mg) were pooled, dialyzed against TB/75 mM KCl, and applied to a Ø1.0 cm×1.0 cm column of single-stranded DNA (ssDNA) cellulose equilibrated in TB/75 mM KCl. The ssDNA column was washed with TB/75 mM KCl, and eluted with a linear gradient of TB/75 mM KCl to TB/750 mM KCl. Ku-eGFP eluted at approximately 270 mM KCl (40 fractions of 0.75 mL). Ku-eGFP was resolved by SDS-PAGE, immunoblotting, and Coomassie blue staining.

Ku-eGFP containing fractions from ssDNA cellulose column (total protein 0.75 mg) were pooled, dialyzed against TB/75 mM KCl containing 0.02% (*v*/*v*) Tween-20 (TBT), and applied at a flow rate of 1 mL min^{-1} to a 1 mL MonoQ HR5/50 GL FPLC column (UNICORN 4.11, Amersham Bioscience) pre-equilibrated in TBT/75 mM KCl. The MonoQ column was washed with TBT/75 mM KCl and eluted with a controlled linear gradient of TBT/75 mM KCl to TBT/750 mM KCl over 90 min. Ku-eGFP eluted at approximately 240 mM KCl (100 fractions of 0.5 mL). The presence of Ku-eGFP in column fractions was resolved by SDS-PAGE and immunoblotting.

Fractions containing purified Ku-eGFP were pooled (final yield of 23 μg), concentrated (0.33 μM) using a VivaSpin 15R (5000 MWCO, Sartorius AG), aliquoted, frozen in liquid nitrogen, and stored at −80 °C. Because of potential photosensitivity, Ku-eGFP was stored protected from light.

DNA-PK autophosphorylation assay: Purified Ku-eGFP (0.25 μg) or Ku (0.25 μg) was preincubated alone, or in the presence of DNA-PKcs (0.75 μg) at 30 °C for 20 min in reaction buffer [25 mM Hepes pH 7.5, 75 mM KCl, 10 mM $MgCl_2$, 0.1 mM EDTA, 0.2 mM EGTA], plus sonicated calf thymus DNA (CT-DNA; Fluka; 10 μg mL^{-1}), DTT (1 mM), and ATP (0.25 mM) to a final volume of 20 μL. The reaction was initiated by ATP. Where indicated, wortmannin (WM; 150 nM final concentration) was preincubated with DNA-PKcs for 15 min prior to being added to the reaction. Purified DNA-PKcs was a generous gift from Prof. Dr. David Chen, University of Texas Southwestern Medical Center. Wild-type (wt) Ku heterodimer used for control experiments was purified from HeLa SS6 cells as described above for Ku-eGFP.

Immunoblotting: Ku-eGFP samples and kinase assay samples were resolved by 8% SDS-PAGE, and transferred to nitrocellulose at 100 V for 60 min in electroblot buffer [48 mM Tris-HCl, 39 mM glycine, 20% (*v*/*v*) methanol]. A mouse monoclonal antibody to human Ku80 (ab2173, Abcam) was used to identify Ku80eGFP. Ku-eGFP heterodimer was also probed by immunoblotting with a rabbit polyclonal antibody to hamster Ku70 (ab10878, Abcam) and by rabbit polyclonal antibody against eGFP (ab290, Abcam). Phosphorylated DNA-PKcs was probed by a phosphospecfic mouse monoclonal antibody specific to phosphothreonine (Thr) 2609 of DNA-PKcs (ab18356, Abcam).

Confocal microscopy and fluorescence correlation spectroscopy (FCS): Cell imaging and FCS was performed using a commercial ConfoCor 2 laser scanning microscope (LSM; Zeiss, Jena, Germany) with an argon ion laser (488 nm, 25 mW, at 18% of maximum power output). A Zeiss C-Apochromat water immersion objective 40×, NA = 1.2 (Zeiss) was used with an adjustable pinhole set at 70.5 μm to ensure a confocal geometry. A band-pass filter transmitting 505–550 nm (Zeiss) was used to separate the eGFP fluorescence signal. In order to avoid saturation of the fluorescence intensity in the scanned images the detector settings were optimized by using the range indicator feature provided by the Zeiss software [Operating Manual LSM510, Zeiss, Jena, Germany]. FCS measurements were performed by epi-illuminating the sample with the 488-nm Ar laser ($I_{ex} \approx 1.2$ kW cm^{-2}). The excitation light was reflected by a dichroic mirror (HTF 488) and focused onto the sample by the same objective as for the LSM. The fluorescence emission was recollected back and sent to an avalanche photodiode via a 505–530 nm bandpass filter. Out-of-plane fluorescence was reduced by a pinhole (90 μm) in front of the detector. The laser focus was positioned either within the cell nucleus or cytoplasm away from the plasma membrane or nuclear envelope, or within a buffered solution containing either free purified Ku-eGFP, eGFP, or AlexaFluor488 (Invitrogen). The fluorescence temporal signal was recorded and the autocorrelation function $G(\tau)$ was calculated according to ref. [44]. The apparatus was calibrated prior to each experiment by measuring the known three-dimensional diffusion coefficient of AlexaFluor 488 (Invitrogen) in solution (4.14×10^{-10} m^2s^{-1}).[45] The detection area on the focal plane was approximated to a Gaussian profile and had a radius of $\approx$ 0.20 μm at $1e^{-2}$ relative intensity. Data fitting was performed with the Levenberg-Marquardt nonlinear least-squares fit algorithm (ORIGIN, OriginLab, Northampton, MA). The fitting equation made use of a two-dimensional Brownian diffusion model, assuming a Gaussian beam profile [Eq. (2)]:

$$G(\tau) = \frac{\sum_i \langle C_i \rangle [1/(1+\tau/\tau_{d,i})]}{A_{\text{eff}} (\sum_i \langle C_i \rangle)^2} \quad (2)$$

where $\langle C_i \rangle$ is the two-dimensional time average concentration of the species *i* in the detection area A_{eff} and $\tau_{d,i}$ is the average residence time of the species *i*. The diffusion coefficient D_i for the species *i* is inversely proportional to $\tau_{d,i}$. For cellular FCS measurements, only one measurement per cell nucleus or cytoplasm was performed with one measurement defined as the average of ten acquisition rounds of 10 s, to minimize the effects of photobleaching. The corresponding average correlation curve was exported to Microcal Origin and the data fit as described above.

Laser induced DNA damage in cells: A home-built setup was established and consisted of 1) a Mira Optima 900-F (Coherent) two-photon laser with 800-nm wavelength, 76 MHz repetition rate of

the pulses, 150 fs duration per pulse; 2) a beam expander; 3) the neutral density filter (OD = 1.4); and 4) a microscope (Olympus IX 71) including a dichroic mirror and a water immersed 60×IR/1.2 NA objective (Olympus UPlanApo). The focused laser beam has a focal volume of approximately 0.24 fL.

The two-photon laser, with a power of 4.38 mW, was moved linearly across the nucleus of cells to form DSBs shown as Ku-eGFP localized stripes later under fluorescent light (each cell nucleus was illuminated for approximately 5–10 s). Laser damaged cells were imaged as described above. No trace of laser damage was visible using differential interference contrast (DIC) microscopy, and could only be visualized by Ku-fluorescence localization in the nucleus. The laser power was of the order of 5.1×10^{-6} J per pulse (approximately 1.4 MW cm^{-2}).

Microinjection: Purified Ku-eGFP was concentrated (to 6.1 μM) by Microcon YM-3 spin tubes (MWCO = 3000 Da, MilliPore). Ku-eGFP was loaded in the micropipette (Femtotip 2, Eppendorf) and injected into the cytoplasm of HeLa SS6 cells as previously described.[46] The micromanipulator consists of a FemtoJet and InjectMan NI2 (Eppendorf) which was mounted directly on an Olympus microscope IX-71. Working pressure for injection in adherent cells was between 45–90 hPa for 0.1 s and a holding pressure of 35–40 hPa.

Acknowledgements

The authors wish to sincerely thank Prof. David Chen at the University of Texas Southwestern Medical Center for supplying purified DNA-PKcs and to Prof. W. Rodgers of the Oklahoma Medical Research Foundation for supplying the pWay20Ku80eGFP and Ku70eGFP constructs. Also thanks to Elke Haustein, Jörg Mütze, Jonas Ries, and Anke Bohrmann for providing assistance with the home built two-photon laser set-up, assistance in FCS curve fitting, and for assistance with the preparation of the pEGFP-C2-Ku80 construct. The authors would also like to thank Drs. N. Kahya, A. A. Goodarzi, Geddy Lee, and W. D. Block for critical discussions regarding the manuscript. D.M. is grateful to the Alexander von Humboldt foundation for a fellowship supporting this work.

Keywords: DNA double-strand-break repair · DNA-PK · fluorescence correlation spectroscopy · Ku heterodimer · nonhomologous end-joining

[1] S. P. Lees-Miller, K. Meek, *Biochimie.* **2003**, *85*, 1161–1173.
[2] K. Meek, S. Gupta, D. A. Ramsden, S. P. Lees-Miller, *Immunol. Rev.* **2004**, *200*, 132–141.
[3] J. R. Walker, R. A. Corpina, J. Goldberg, *Nature* **2001**, *412*, 607–614.
[4] J. Paupert, S. Dauvillier, B. Salles, C. Muller, *EMBO Rep.* **2007**, *8*, 583–588.
[5] S. Monferran, J. Paupert, S. Dauvillier, B. Salles, C. Muller, *EMBO J.* **2004**, *23*, 3758–3768.
[6] S. Monferran, C. Muller, L. Mourey, P. Frit, B. Salles, *J. Mol Biol.* **2004**, *337*, 503–511.
[7] Y. Munakata, T. Saito-Ito, K. Kumura-Ishii, J. Huang, T. Kodera, T. Ishii, Y. Hirabayashi, Y. Koyanagi, T. Sasaki, *Blood.* **2005**, *106*, 3449–3456.
[8] B. Kysela, A. J. Doherty, M. Chovanec, T. Stiff, S. M. Ameer-Beg, B. Vojnovic, P. M. Girard, P. A. Jeggo, *J. Biol. Chem.* **2003**, *278*, 22466–22474.
[9] J. S. Kim, T. B. Krasieva, H. Kurumizaka, D. J. Chen, A. M. Taylor, K. Yokomori, *J. Cell Biol.* **2005**, *170*, 341–347.
[10] D. Merkle, W. D. Block, Y. Yu, S. P. Lees-Miller, D. T. Cramb, *Biochemistry.* **2006**, *45*, 4164–4172.
[11] P. O. Mari, B. I. Florea, S. P. Persengiev, N. S. Verkaik, H. T. Bruggenwirth, M. Modesti, G. Giglia-Mari, K. Bezstarosti, J. A. Demmers, T. M. Luider, A. B. Houtsmuller, D. C. van Gent, *Proc. Natl. Acad. Sci. USA* **2006**, *103*, 18597–18602.
[12] N. Uematsu, E. Weterings, K. Yano, K. Morotomi-Yano, B. Jakob, G. Taucher-Scholz, P. O. Mari, D. C. van Gent, B. P. Chen, D. J. Chen, *J. Cell Biol.* **2007**, *177*, 219–229.
[13] F. Chen, S. R. Peterson, M. D. Story, D. J. Chen, *Mutat. Res.* **1996**, *362*, 9–19.
[14] B. K. Singleton, A. Priestley, H. Steingrimsdottir, D. Gell, T. Blunt, S. P. Jackson, A. R. Lehmann, P. A. Jeggo, *Mol. Cell. Biol.* **1997**, *17*, 1264–1273.
[15] M. Koike, A. Koike, *J. Radiat. Res. (Tokyo).* **2004**, *45*, 119–125.
[16] G. E. Taccioli, T. M. Gottlieb, T. Blunt, A. Priestley, J. Demengeot, R. Mizuta, A. R. Lehmann, F. W. Alt, S. P. Jackson, P. A. Jeggo, *Science* **1994**, *265*, 1442–1445.
[17] V. Smider, W. K. Rathmell, M. R. Lieber, G. Chu, *Science* **1994**, *266*, 288–291.
[18] G. L. Chen, L. Yang, T. C. Rowe, B. D. Halligan, K. M. Tewey, L. F. Liu, *J. Biol. Chem.* **1984**, *259*, 13560–13566.
[19] T. M. Gottlieb, S. P. Jackson, *Cell* **1993**, *72*, 131–142.
[20] D. W. Chan, C. H. Mody, N. S. Ting, S. P. Lees-Miller, *Biochem. Cell Biol.* **1996**, *74*, 67–73.
[21] M. Koike, T. Ikuta, T. Miyasaka, T. Shiomi, *Oncogene.* **1999**, *18*, 7495–7505.
[22] M. Koike, T. Ikuta, T. Miyasaka, T. Shiomi, *Exp Cell Res.* **1999**, *250*, 401–413.
[23] J. S. Kim, T. B. Krasieva, V. LaMorte, A. M. Taylor, K. Yokomori, *J. Biol. Chem.* **2002**, *277*, 45149–45153.
[24] Y. Nomura, H. Tanaka, L. Poellinger, F. Higashino, M. Kinjo, *Cytometry.* **2001**, *44*, 1–6.
[25] Y. Chen, J. D. Muller, Q. Ruan, E. Gratton, *Biophys. J.* **2002**, *82*(1), 133–144.
[26] A. A. Goodarzi, S. P. Lees-Miller, *DNA Repair (Amst).* **2004**, *3*, 753–767.
[27] D. W. Chan, B. P. Chen, S. Prithivirajsingh, A. Kurimasa, M. D. Story, J. Qin, D. J. Chen, *Genes Dev.* **2002**, *16*, 2333–2338.
[28] K. Bacia, S. A. Kim, P. Schwille, *Nat. Methods* **2006**, *3*, 83–89.
[29] K. Bacia, P. Schwille, *Nat. Protoc* **2007**, *2*, 2842–2856.
[30] S. A. Kim, K. G. Heinze, P. Schwille, *Nat. Methods* **2007**, *4*, 963–73.
[31] J. Ries, P. Schwille, *Biophys J.* **2006**, *91*, 1915–1924.
[32] N. O. Petersen, P. L. Hoddelius, P. W. Wiseman, O. Seger, K. E. Magnusson, *Biophys. J.* **1993**, *65*, 1135–1146.
[33] M. Srivastava, N. O. Petersen, *Methods Cell Sci.* **1996**, *18*, 47–54.
[34] J. R. Lakowicz, *Principles of Fluorescence Spectroscopy*, 3rd ed., Springer, Berlin, **2006**.
[35] U. Meseth, T. Wohland, R. Rigler, H. Vogel, *Biophys. J.* **1999**, *76*, 1619–1631.
[36] P. Schwille, U. Haupts, S. Maiti, W. W. Webb, *Biophys. J.* **1999**, *77*, 2251–2265.
[37] M. Giampuzzi, G. Botti, M. Di Duca, L. Arata, G. Ghiggeri, R. Gusmano, R. Ravazzolo, A. Di Donato, *J. Biol. Chem.* **2000**, *275*, 36341–36349.
[38] H. L. Hsu, D. Gilley, S. A. Galande, M. P. Hande, B. Allen, S. H. Kim, G. C. Li, J. Campisi, T. Kohwi-Shigematsu, D. J. Chen, *Genes Dev.* **2000**, *14*, 2807–2812.
[39] T. S. Fisher, V. A. Zakian, *DNA Repair (Amst).* **2005**, *4*, 1215–1226.
[40] A. I. Walker, T. Hunt, R. J. Jackson, C. W. Anderson, *EMBO J.* **1985**, *4*, 139 – 145.
[41] S. P. Lees–Miller, Y. R. Chen, C. W. Anderson, *Mol. Cell. Biol.* **1990**, *10*, 6472–6481.
[42] L. Fang, Y. Wang, D. Du, G. Yang, T. T. Kwok, S. K. Kong, B. Chen, D. J. Chen, Z. Chen, *Cell Res.* **2007**, *17*, 572–574.
[43] D. Arosio, S. Costantini, Y. Kong, A. Vindigni, *J. Biol. Chem.* **2004**, *279*, 42826–42835.
[44] D. Magde, E. Elson, W. W. Webb, *Phys. Rev. Lett.* **1972**, *29*, 705–708.
[45] E. P. Petrov, T. Ohrt, R. G. Winkler, P. Schwille, *Phys. Rev. Lett.* **2006**, *97*, 258101.
[46] T. Ohrt, D. Merkle, K. Birkenfeld, C. J. Echeverri, P. Schwille, *Nucleic Acids Res.* **2006**, *34*, 1369–1380.

Received: January 5, 2008
Published online on April 24, 2008

